FLEXURAL QUASI-STATIC BEHAVIOUR OF UHPFRC CIRCULAR SLAB SPECIMENS

Xiujiang Shen (1) and Eugen Brühwiler (1)

(1) Division of Maintenance and Safety of Structures (MCS-ENAC), EPFL, Switzerland

Abstract

This paper investigates experimentally and numerically the biaxial flexural behaviour of thin circular slab specimens made of Ultra High Performance Fibre Reinforced Cementitious Composite (UHPFRC). The circular slab specimens represent an external tensile reinforcement layer for reinforced concrete (RC) slabs or a new thin slab element, for the application, e.g. in bridge construction. The ring-on-ring test method has been developed to measure the equi-biaxial strength and deflection of the specimens. The 3-D deformation field and crack development on tensile surface are recorded continually using Digital Image Correlation (DIC). The experimental results validate the ring-on-ring test method, allowing for the consideration of the stochastic nature of UHPFRC. Significant flexural and deformational capacities of UHPFRC slab under biaxial condition are highlighted. Furthermore, 3-D non-linear finite-element analysis (FEA) accurately simulates the structural behaviour of the tested slabs.

Résumé

Cet article étudie expérimentalement et numériquement le comportement en flexion bi-axiale de dalles circulaire minces en composite cimentaire fibré à ultra-hautes performances (BFUP). Ces éprouvettes de dalles circulaires représentent une couche de renfort externe en traction pour des dalles de béton armé, ou une dalle mince neuve, destinée par exemple à la construction de ponts. La méthode d'essai anneau-sur-anneau a été développée pour mesurer la résistance et la flexion des éprouvettes sous sollicitation équi-biaxiale. Le champ de déformations 3-D et le développement des fissures sur la surface tendue sont mesurés en continu par analyse d'images. Les résultats expérimentaux valident la méthode de test anneau sur anneau, ce qui permet de prendre en considération la nature stochastique du BFUP. Les capacités de résistance en flexion et de déformation importantes de la dalle en BFUP sous condition bi-axiales sont mises en évidence. De plus, l'analyse aux éléments finis non linéaires 3-D simule avec précision le comportement structurel des dalles testées.

1. INTRODUCTION

Ultra-High Performance Fiber Reinforced Cementitious Composites (UHPFRC) are composed of a very compact cementitious matrix and a high amount of slender steel fibers. UHPFRC possesses extremely low permeability, high ductility and high strength (compressive strength $\geq 180 MPa$, tensile strength $\geq 10 MPa$), characterized by a strain-hardening and softening behavior in tension (Fig.1a).

Application of UHPFRC to specific zones of structural members under severe mechanical and environmental actions has proven to be an effective method to improve (strengthen) structural members [1]. The original concept of placing UHPFRC or R-UHPFRC on the top surface of reinforced concrete (RC) after preparation of the substrate surface by water jetting has been developed and validated by means of more than 15 years of research and site applications, as illustrated in Fig 1(b). This technology combines the resistance and protection properties of UHPFRC and has the general objective to significantly improve structural resistance and durability [2, 3].
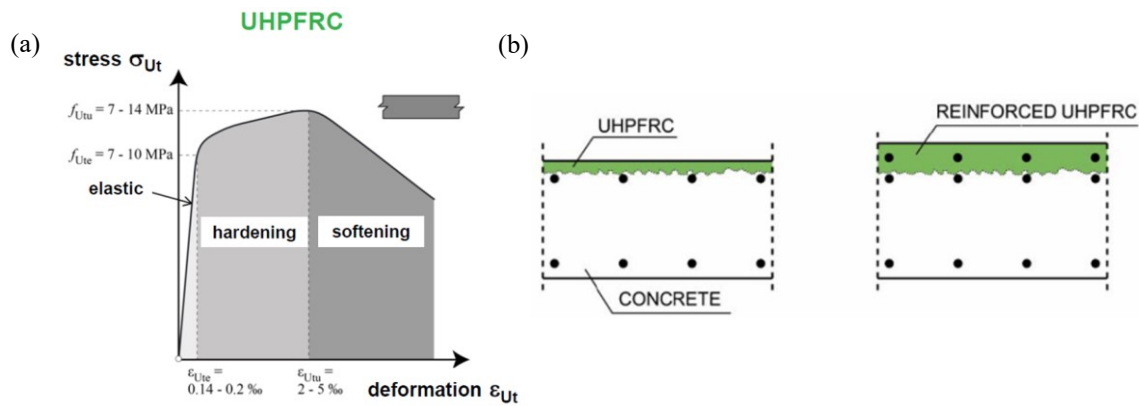

Figure 1 (a) Tensile response of UHPFRC (b) Application of UHPFRC as strengthening layer [3]

In the case of bridge deck slabs, the most severely loaded structural elements in bridges, the actual stress state caused by wheel loading is nearly equi-biaxial [4]. In this context, comprehensive understanding of the structural behavior of bridge deck slabs under biaxial conditions is essential in the design and examination processes, when UHPFRC or R-UHPFRC is applied to strengthen existing structural elements in RC or steel or as new slabs made of R-UHPFRC.

The ring-on-ring test, as an extended 3D version of the four-point bending test, is composed of a support ring, concentric loading ring and circular specimen. It has been extensively adopted and even standardized by ASTM [5] in the ceramics and glass domain. Recently, this method was modified and validated to measure the biaxial flexure strength of concrete [6–8]: This adapted ring-on-ring test yielded stable test results with small variation, thereby appearing to be a reliable and practical means of determining biaxial tensile strength of concrete. Additionally, a modified equation for calculation of biaxial tensile strength of concrete was proposed based on the plate bending theory, shown in Eq. (1).

$$\sigma_b = \frac{3P}{4\pi h^2}\left\{(1-v)\left[1-\left(\frac{b}{a}\right)^2\right]-2(1-v)\ln(\frac{b}{a})\right\} \qquad (1)$$

The application of this biaxial flexural test method has been extended to UHPFRC by several researchers [9,10]. The test results show that the ring-on-ring test allowed the actual development of fiber bridging effect between cracks, accurately representing the behavior of UHPFRC members subjected to biaxial flexural loading. Furthermore, higher equivalent flexural tensile strength and energy absorption as well as lower scatter results were observed from the biaxial flexure tests than those from 4-point bending test or central loading test.
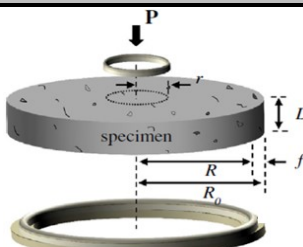
Accordingly, the aim of this paper is to investigate the flexural behavior of UHPFRC under biaxial stress state by means of an experimental program and finite element analysis. Using the ring-on-ring test method, biaxial flexural tests have been conducted on three slab-like specimens without conventional reinforcement, as representative elements of a bridge deck slab.

2. EXPERIMENTAL PROGRAM

2.1 Test specimens and preparation

The chosen UHPFRC is Holcim 707 (H707), an industrial premix containing 3.8 % by volume of 13 mm long straight steel fibers with diameter of 0.175 mm. The test was carried out on a circular slab with R = 600mm and thickness D = 50mm.

Table 1. Summary of test program

Test Method	Geometry	Reinforcement Ratio	Number of specimens
	Circular slab (R = 600mm, D = 50mm, r = 150mm, R_0 = 500mm)	0	3 UHPFRC slab (S1-1, S1-2, S1-3)

The specimens were cast in one step: the fresh UHPFRC (workability t_{600} = 11.1 s) was placed at the center and let flown without pulling or vibration (Fig. 2).

Once the casting was completed, a plastic sheet was pulled over the specimens to allow for auto-curing of the material. The formwork was removed 24 hours after the casting. The slabs were then kept under moist curing conditions for the following seven days, and sequentially, stored inside the laboratory until testing.
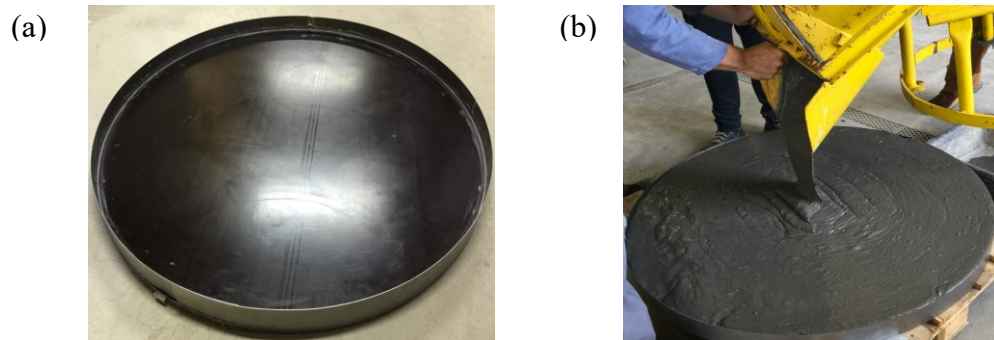
(a)   (b)

Figure 2 (a) Formwork for casting a circular slab and (b) casting procedure

2.2 Test method and procedure

Ring-on-ring test method was applied for flexural testing, Figure 3 shows the full test set-up and devices. The slab was simply supported on a support ring with $R_0 = 500$ mm. Loading was imposed by a hydraulic jack acting on the center of slab through a force transmitting ring with $r = 150$ mm. All the slabs were subjected to three loading–unloading cycles to 20 kN with an actuator displacement rate of 1.0 mm/min. Afterwards, a monotonic loading with same displacement rate was applied up to the peak force, followed by a rate of 4.0 mm/min until the actuator displacement reached 80mm. A force cell installed between the jack and the specimen was used to monitor the force with frequency of 5 Hz.

The slabs were tested with the casting surface facing up, allowing the observation of tensile crack propagation on the smooth surface. Before testing, the casting surface was polished by hand-held grinding machine and a mortar layer was placed between support ring and bottom surface to level out both surfaces. Two rubber pads (thickness of 10 mm, E = 500 MPa) were positioned between the slab surfaces and the two rings to distribute the force evenly.
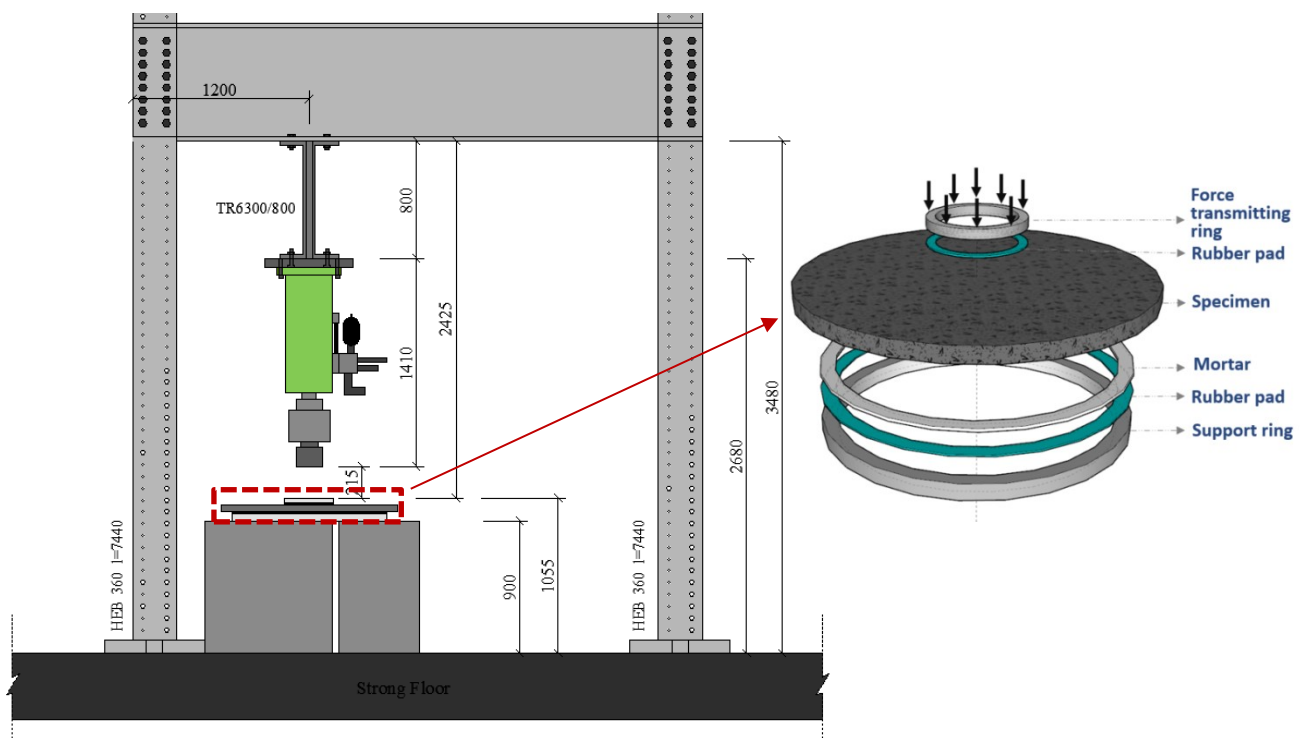

Figure 3. Schematic description of test setup

Digital Image Correlation (DIC) technique was applied to investigate the deflection development, strain field and micro-cracking (Fig.4-b). Two digital cameras were placed underneath the slab at a distance of 0.5m and angle of 23 degrees to the vertical. The slab area, which was visible to DIC, was about Ø 600 mm on the center of the slab. The shooting of the 2 cameras were synchronized via wired computer control with frequency of 0.1 Hz.

There were seven LVDTs and four U4 gages installed on the top surface to measure the deflection and strain, illustrated in Figure 4(a). All deflection measurements were made with respect to the strong floor. The measurement frequency was 5 Hz.
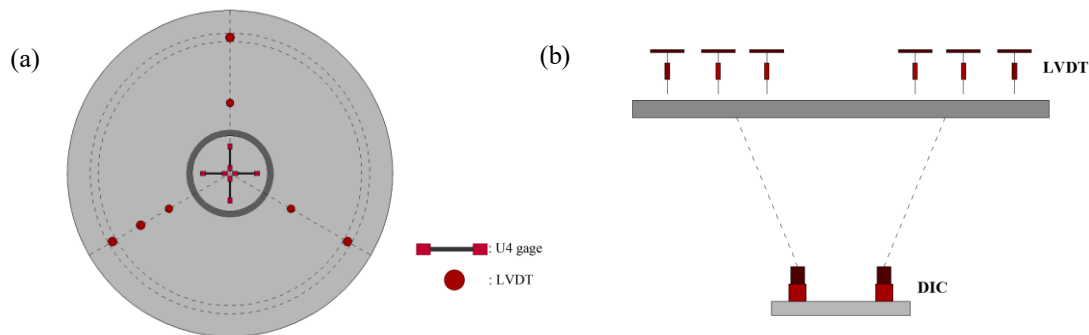
Figure 4. Measurement devices' placement configurations:
(a) compression surface (7 LVDTs and 4 U4 gages); (b) side view (LVDTs and DIC)

3. EXPERIMENTAL RESULTS AND DISCUSSION

3.1 Flexural response

The test results of three slabs are presented in terms of measured force vs. deflection of the centre point, as shown in Figure 5. The latter was measured by DIC on bottom surface, excluding the deformation of rubber pad measured from three LVDTs on the top surface.

All slabs showed similar flexural response: a linear response was observed at the beginning until first fine microcracking was observed at approximately 40~45 kN, and sequentially a clear long deflection hardening behaviour was recorded. The first fine microcrack was detected by the DIC analysis, and was conventionally determined as the end of elasticity. After peak load, the slabs exhibited important post-peak behaviour with high residual resistance with increasing deflection. In the case of S1-2, the residual force is 73 % of the maximum resistance with corresponding deflection of 39.25 mm, and S1-3 presents residual force of 77 % of the maximum resistance with corresponding deflection of 39.85 mm.
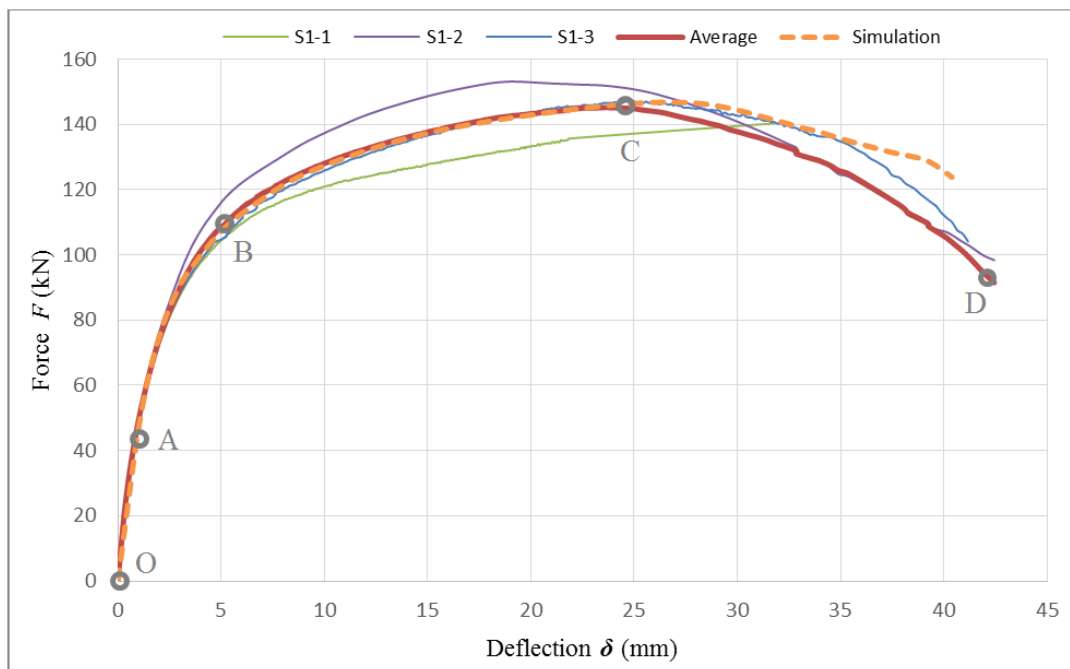

Figure 5. Force-deflection response of each slab

Accordingly, the force-deflection curves from Figure 5 can be classified into four characteristic phases. The first phase is identified as a linear behaviour, dominated by the properties of the matrix (OA). Once microcracking occurs, the curves enter into the second phase with slightly decreasing stiffness, the steel fibers bear increasingly stress through the mechanism of strain compatibility, bonding and debonding. This phase is characterized by more and more pronounced non-linear behaviour with development of multiple microcracking (AB). Afterward, discrete cracks localize and develop with small increase of force. In this third stage, fibers bridging the discrete cracks are debonded and subjected to pull-out mechanism (BC). Finally, a forth phase is distinguished beyond peak force with slight decrease of measured force values due to the loss of bridging effect by fibers (CD).

Table 2. Summary of characteristic parameters of each slab and simulation results

No.	F_{cr}(kN)	δ_{cr}(mm)	F_p(kN)	δ_p(mm)	σ_{cr}(MPa)	σ_p(MPa)	n
S1-1	44.33	0.87	140.34	31.75	12.25	38.79	8
S1-2	41.66	0.77	153.16	19.06	11.52	42.33	7
S1-3	41.49	0.75	147.14	25.01	11.47	40.67	5
Average	42.49	0.80	146.88	25.27	11.75	40.60	
Std. dev.	1.59	0.06	6.41	6.35	0.44	1.77	
CV	0.04	0.08	0.04	0.25	0.04	0.04	
Simulation	45.85	0.98	146.83	26.68	12.67	40.59	12

Table 2 summarizes the characteristic parameters based on the force-deflection response: the force (F_{cr}) and deflection (δ_{cr}) at the first observed microcrack, the peak force (F_p) as maximum specimen resistance and the corresponding deflection (δ_p), as well as the biaxial stresses (σ_{cr} ; σ_p) calculated based on Eq.(1), as indicated as point A and B at Fig.7~9, respectively. It is obvious that the ring-on-ring tests on circular UHPFRC slabs provide high reliability with little scatter for all parameters, except the value of δ_p. For example, the variation of F_{cr} and F_p are limited to only 0.04.

3.2 Cracking process and failure mode as observed by DIC analysis
(1) Cracking pattern

Figure 6 illustrates the final cracking pattern for each slab, in which fine visible microcracks are marked with green lines. All slabs generated large cracking area on bottom surface, characterized by several random localized discrete cracks with multiple fine microcracks between them, and final flexural crack failure is observed for all slabs.

The distribution of the discrete cracks and the fine visible microcracks is random, and the numbers of localized discrete cracks (n) are different from each other (Tab.2). For example, among the three slabs, S1-2 generated the most localized cracks, allowing for higher contribution from fibers to specimen's resistance while it has the least microcracking, preventing thus the development of slab's deflection. This results in the highest value of F_p and the lowest value of δ_p for S1-2.
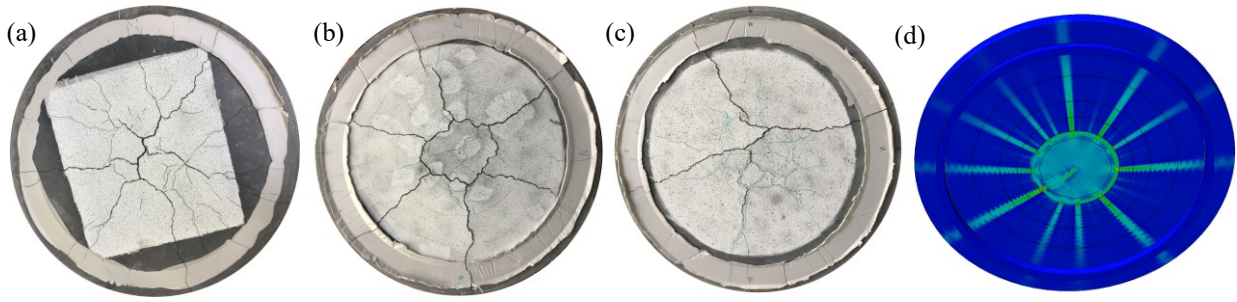
Figure 6. Final crack pattern of (a) S1-1, (b) S1-2, (c) S1-3, (d) simulation

(2) Cracking process

Figures 7 to 9 show the cracking process as observed on the visualized portion (400mm × 400mm) of all slabs at four selected force points with respect to the F-δ curves, namely at around cracking initiation, multiple microcracking development, peak force and formation of discrete cracks. In the case of S1-1, only 3 points could be analyzed. The white dash circle marks the corresponding position of force transmitting ring on slab top surface.

An identical feature for all slabs is that the first fine microcracks initiate within the force transmitting ring area and their directions are random (point A). Afterwards, multiple microcracking behavior with different directions and numbers in the same area is presented (point B), causing stress redistribution. At peak force (C), the localized discrete cracks developed from some of the microcracks observed at (B), and sequentially continued to develop in terms of crack opening with slight decrease of force (D).

Note that the localized discrete cracks are also random in different slabs. These random phenomena of microcracking within the force transmitting ring area may be due to inherent variation in fiber distribution and orientation. Therefore, the ring-on-ring test method considers the stochastic nature of materials, allowing for real development of stress distribution and cracking, which is accurately representative of thin UHPFRC slab elements subjected to biaxial flexural bending.
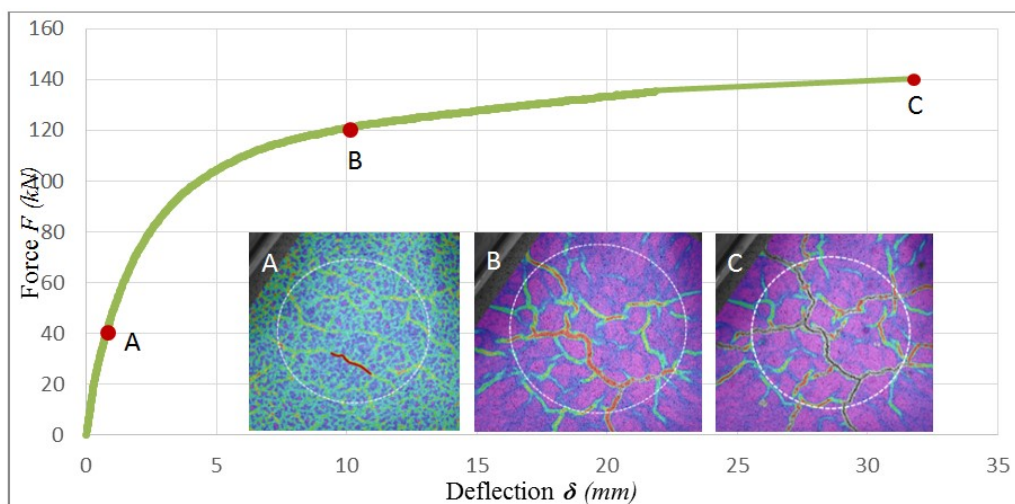

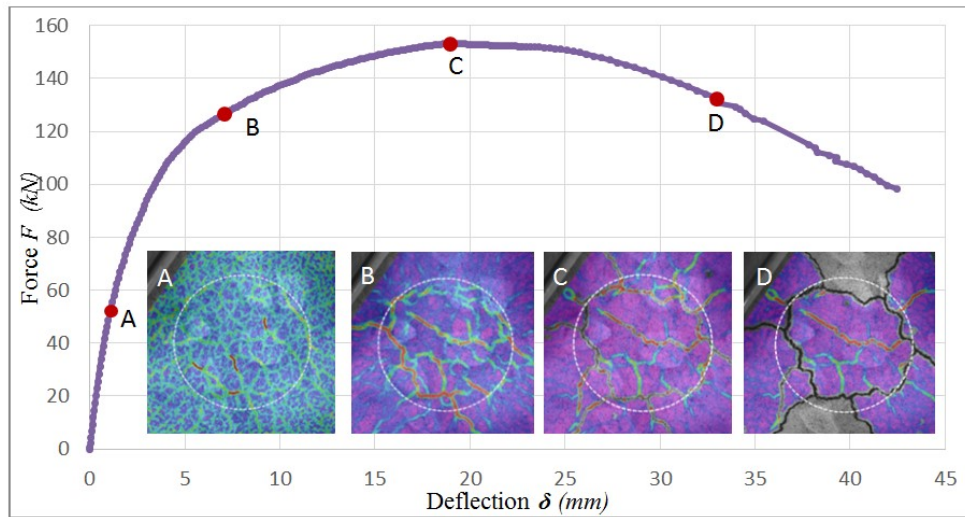Figure 7. Cracking process of S1-1 at different stages

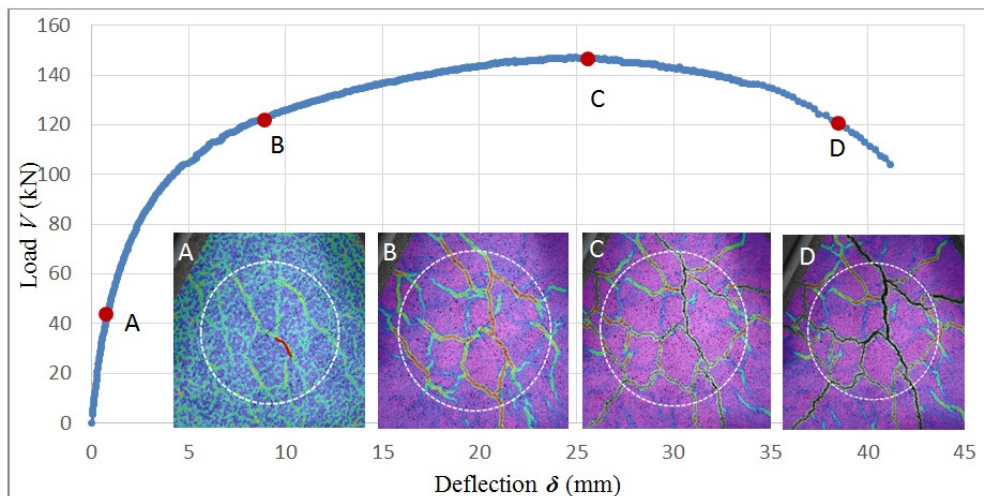Figure 8. Cracking process of S1-2 at different stages

Figure 9. Cracking process of S1-3 at different stages

4. FINITE ELEMENT MODELLING AND ANAYLSIS

A 3-D FE model was built using the non-linear FE analysis software DIANA, targeting at simulating the flexural behavior of the UHPFRC slab in terms of force-deflection response, ultimate resistance and cracking pattern. Considering the random fiber distribution in the slab, the full scale of the slab element was modeled, and the smeared crack concept was adopted.

4.1 Simulation of boundary and loading/support system

The initial simulation used a simple support system in which the incremental loading was applied directly to the nodes on the top surface of the specimens. It resulted in circular local crack on top at the loading position due to stress concentration at the beginning. This is not what was observed in the tests. Therefore, the rubber pads were explicitly modelled by finite elements, made of elastomer with modulus of elasticity of 500MPa and Poisson's ratio of 0.49, then loading was applied on the nodes of rubber pads.

The boundary conditions in simulation of ring-on-ring test have a strong influence on the stability of the numerical procedure and on the fracture pattern. During testing, the specimens were not prevented from sliding and lifting from the supporting ring along fracture growth. Therefore, the two adjacent ¼ points of the support ring were only constrained in tangential directions, and the top surface central point was constrained in both X and Y directions. Additionally, the interface elements were built between the specimen and the rubber pads, avoiding tensile reaction force from the supporting ring.

4.2 Constitutive model for UHPFRC

Based on the previous study from uniaxial direct tensile tests on the tested UHPFRC material [11], a simplified tensile constitutive law with a bilinear ascending elastic-hardening branch and a bilinear descending softening branch was adopted for circular slabs in DIANA model. UHPFRC mechanical properties include: $f_{Ut,el}$=9.5MPa (elastic limit stress), $f_{Ut,u}$=11MPa (tensile strength), $\varepsilon_{Ut,u}$=0.2% (maximum hardening deformation), $f_{Ut,Sl}$=3MPa (stress at the breaking point of the bilinear softening law) and $w_{U,l}$=0.45%l_{ch} (maximum discrete crack opening) and E_U=47.5GPa (modulus of elasticity).

4.3 Comparison between numerical and experimental results

The comparison of F-δ curves between numerical simulation results and experimental results is shown in Figure 5, where close agreement is noted. The simulation curve almost coincides with the average experimental curve before the peak force, although a slight difference increases in the softening phase. This difference results from different patterns of localized cracks: the number of localized discrete cracks observed on the specimens ranges from 5 to 8, while 12 cracks localise in the simulation, allowing for more contribution from fiber bridging effects (mainly pull-out effects) to residual resistance after peak force. Thus, the softening curve in the simulation displays a flatter response with less loss of stiffness compared with experimental curves. Also, more fibers were pulled out with increasing deflection, ultimately resulting in increasing difference after peak force.

Regarding the cracking process and pattern, the results from numerical simulation and testing are similar, as shown in Figure 6. However, more significant multiple microcracking is observed within the force transmitting area of the bottom slab surface in the simulation, as well as more localized discrete cracks, as mentioned before. This is because of the assumption of the uniform material properties in the FE model which is only an approximation of real UHPFRC properties.

The most important results from the numerical simulation are summarized in Table 2: the ultimate resistance (maximum force) and corresponding deflection are predicted precisely, while a slightly higher force value for first microcracking (45.85kN) is obtained in simulation compared to the test (42.49kN).

5.　CONCLUSIONS

This paper presents an investigation on the flexural behaviour of UHPFRC slabs under biaxial stress condition through ring-on-ring test method and numerical simulation. The experimental and numerical studies have highlighted the following findings:
- The ring-on-ring test method on circular UHPFRC slabs shows small scatter in test results, and allows for the implicit consideration of the stochastic nature of UHPFRC properties, representative of thin UHPFRC slab elements.
- The tested slab elements exhibited similar biaxial flexural behaviour in terms of force-deflection response that was classified into four phases, namely elastic phase, microcracking

initiation and multiple microcracking phase, multiple discrete cracking phase and softening phase. Significant flexural and deformational capacities are noted.

– Regarding cracking patterns, the first microcrack initiates randomly within the force transmitting ring area on the bottom surface of the UHPFRC slab, followed by pronounced multiple microcracking. The number of localized discrete cracks for all slabs range from 5 to 8. The direction and distribution of microcracks and discrete cracks are random depending on fiber orientation and distribution in each slab element, thus producing some variation in flexural response after peak. Such variation increases gradually with increasing discrete crack opening.

– The 3-D non-linear FEA accurately simulates the structural behaviour of the tested slab elements in terms of force-deflection response, ultimate resistance and crack patterns. The simulation also confirms that the failure is governed by the flexural mode, as observed experimentally.

REFERENCES

[1] Brühwiler E. Rehabilitation and strengthening of concrete structures using ultra-high performance fibre reinforced concrete. Concrete Repair, Rehabilitation and Retrofitting III: 3rd International Conference on Concrete Repair, Rehabilitation and Retrofitting, ICCRRR-3, 3-5 September 2012, Cape Town, South Africa, CRC Press; 2012, p. 30.

[2] Denarié E, Brühwiler E. Cast-on site UHPFRC for improvement of existing structures–achievements over the last 10 years in practice and research. 7th workshop on High Performance Fiber Reinforced Cement Composites, 1-3, June 2015, Stuttgart, Germany, 2015.

[3] Brühwiler E. "Structural UHPFRC": Welcome to the post-concrete era! First International Interactive Symposium on UHPC - 2016.

[4] Kim J, Kim DJ, Park SH, Zi G. Investigating the flexural resistance of fiber reinforced cementitious composites under biaxial condition. Composite Structures 2015;122:198–208.

[5] ASTM C. 1499-05. Standard test method for monotonic equibiaxial flexural strength of advanced ceramics at ambient temperature. ASTM International, West Conshohocken, Pennsylvania 2009.

[6] Zi G, Oh H, Park S-K. A novel indirect tensile test method to measure the biaxial tensile strength of concretes and other quasibrittle materials. Cement and Concrete Research 2008;38:751–756.

[7] Ekincioglu O. A discussion of paper "A novel indirect tensile test method to measure the biaxial tensile strength of concretes and other quasibrittle materials" by G. Zi, H. Oh, S.K. Park. Cement and Concrete Research 2010;40:1769–70.

[8] Kim J, Kim DJ, Zi G. Improvement of the biaxial flexure test method for concrete. Cement and Concrete Composites 2013;37:154–160.

[9] Yoo D-Y, Banthia N, Zi G, Yoon Y-S. Comparative Biaxial Flexural Behavior of Ultra-High-Performance Fiber-Reinforced Concrete Panels Using Two Different Test and Placement Methods. Journal of Testing and Evaluation 2017;45:20150275.

[10] Yoo D-Y, Zi G, Kang S-T, Yoon Y-S. Biaxial flexural behavior of ultra-high-performance fiber-reinforced concrete with different fiber lengths and placement methods. Cement and Concrete Composites 2015;63:51–66.

[11] Bastien-Masse M, Denarié E, Brühwiler E. Effect of fiber orientation on the in-plane tensile response of UHPFRC reinforcement layers. Cement and Concrete Composites 2016;67:111–25.